



HAL
open science

A comparison of a one-dimensional finite element method and the transfer matrix method for the computation of wind music instrument impedance

Robin Tournemenne, Juliette Chabassier

► To cite this version:

Robin Tournemenne, Juliette Chabassier. A comparison of a one-dimensional finite element method and the transfer matrix method for the computation of wind music instrument impedance. 2019. hal-01963674v1

HAL Id: hal-01963674

<https://inria.hal.science/hal-01963674v1>

Preprint submitted on 21 May 2019 (v1), last revised 24 Oct 2019 (v2)

HAL is a multi-disciplinary open access archive for the deposit and dissemination of scientific research documents, whether they are published or not. The documents may come from teaching and research institutions in France or abroad, or from public or private research centers.

L'archive ouverte pluridisciplinaire **HAL**, est destinée au dépôt et à la diffusion de documents scientifiques de niveau recherche, publiés ou non, émanant des établissements d'enseignement et de recherche français ou étrangers, des laboratoires publics ou privés.

A comparison of a one-dimensional finite element method and the transfer matrix method for the computation of wind music instrument impedance

Robin Tournemenne¹⁾, Juliette Chabassier¹⁾

¹⁾ Magique 3D Team, Inria Bordeaux Sud Ouest, 200 avenue de la vieille tour, 33405 Talence Cedex, France, firstname.lastname@inria.fr

1 Summary

This work presents a computation tool for the calculation of wind instrument input impedance in the context of linear planar wave propagation with viscothermal losses. The originality of the approach lies in the usage of a specific finite element method (FEM) which has a simple implementation given the one dimensional nature of the problem. The results can be arbitrarily precise and any instrument geometry can be computed. The popular Transfer Matrix Method (TMM) is also recalled and a seamless mathematical formulation of its expression is proposed which does not distinguish the cases cylinders vs. cones. In presence of viscothermal losses and for conical parts, the method is not exact and the equation which is exactly solved is exhibited. The accuracy of the two methods (FEM and TMM) and the associated computation times are assessed and compared. Although the TMM is more efficient in lossless cases and for lossy cylinders, the FEM is shown to be more efficient when targeting a specific precision in the realistic case of a lossy trumpet. Unusual physical situations are also possible to solve. All the results of this article are computed using the open-source python toolbox OpenWind.

1 Introduction

The input impedance of wind instruments is defined as its frequency dependent linear response to an input excitation. This physical quantity is of considerable advantage in understanding the instrument's playing quality, and eventually its musical behavior [Campbell(2004), Chaigne and Kergomard(2016)]. The impedance is used for various purposes, such as the analysis of the instrument's playing properties, the synthesis of their sounds and the design of their shape. Indeed, many studies try to correlate the impedance features to the instrument actual intonation, stability, tone [Backus(1976), Braden *et al.*(2009), Campbell(2004)]. Many syn-

thesis methods rely on the input impedance knowledge to produce realistic sounds [Silva *et al.*(2014)], in order to assess the quality of the physical model, or to provide musicians with virtual instruments. Wind instrument design is the goal of many current initiatives, which try to either reconstruct bores, solve inverse problems based on their measured input impedance [Kausel(2001)], improve existing instruments [Tournemenne *et al.*(2017)] or even develop new instruments [Buys *et al.*(2017)] to fulfill the aspirations of musicians.

On the one hand, since the pioneering work of Webster [Webster(1947)], many methods can measure the input impedance with varying precision and frequency range [Le Roux *et al.*(2008), Caussé *et al.*(1984), Sharp *et al.*(2011)]. On the other hand, physical models associated with computation methods can be used to calculate the input impedance. The current reference computation method is the transfer matrix method (TMM), which has been used in the context of wind instruments for more than 40 years [Plitnik and Strong(1979), Mapes-Riordan(1993)]. The underlying physical model can assume plane or spherical wave propagation in the pipe, mono or multi-modal propagation, viscothermal losses at the pipe walls and a radiation impedance at the pipe output, etc.

The objective of this paper is to propose a new method for the computation of the input impedance, which could noticeably facilitate and broaden numerical instrument design approaches. It is not our purpose in this article to discuss the physical model and especially the validity of the underlying physical assumptions. Although this topic is of great interest, and must rely on precise simulation / measurement comparisons, the present work only focuses on technical aspects of the impedance computation. The methodology is here presented in the simplest possible realistic acoustical case, but the present article will serve as a basis to consider more general physical models in the future. We will present a new computation approach based on a one-dimensional finite element method used on the Telegraph equations with viscothermal losses. No-

85 tice first that, compared to the TMM, the proposed
 86 approach is therefore simply another way of solv-
 87 ing the same equations. Notice also that the objec-
 88 tive is not to solve the acoustical equations in 3D
 89 [Lefebvre and Scavone(2012)], nor the Navier-Stokes
 90 equations in 3D [Giordano(2014)]. The method pro-
 91 posed in this paper is close to finite difference methods
 92 [Bilbao(2009), van den Doel and Ascher(2008)], even
 93 if it is used here in the time-harmonic context.

94 This article goes in pair with an open-source
 95 Python 3 toolbox, Openwind [OpenWInD], that can
 96 be freely downloaded and used to undertake numer-
 97 ical experiments. After introducing the physical con-
 98 text, the practical aspects of this numerical method
 99 (FEM) are first covered, then the current reference
 100 method, the transfer matrix method, is presented and
 101 discussed. A thorough comparison is made in order to
 102 assess the precision, the performance and the new fea-
 103 tures brought by this one-dimensional finite element
 104 implementation, which is expected to provide the ex-
 105 act same numerical solution as the TMM in the same
 106 physical situation.

107 2 Physics-based model

108 Consider an axisymmetric pipe occupying a domain
 109 $\Omega \subset \mathbb{R}^3 = (Ox, Oy, Oz)$ of slowly varying cross section
 110 S and rigid walls developing along the x axis, filled
 with air, see Figure 1.

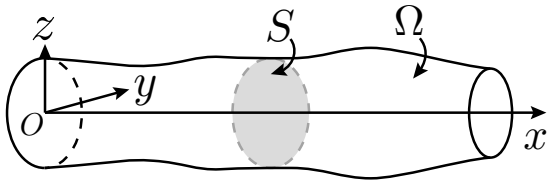


Figure 1: Definition of the space variables. S is the slowly varying section of the axisymmetric pipe.

111
 112 The acoustic pressure $p(x, y, z, t)$ and the three-
 113 dimensional flow $u(x, y, z, t)$ can be considered as
 114 the solution to Navier-Stokes three-dimensional
 115 equations which induce an undue computa-
 116 tional burden in the context where only the
 117 wave propagating phenomena are of interest.
 118 Following the simplifications of Kirchhoff's the-
 119 ory regarding visco-thermal losses near the pipe
 120 walls [Kirchhoff(1868), Zwikker and Kosten(1949),
 121 Chaigne and Kergomard(2016)], the pressure can
 122 be considered as constant in the sections orthog-
 123 onal to the x -axis, the orthogonal components
 124 of the three-dimensional flow can be neglected
 125 in the equations while the axial component can
 126 be considered as axisymmetric with an analytic
 127 expression of its radial dependency. Finally
 128 [Chaigne and Kergomard(2016)], we seek in the

Sound velocity: $c = 331.45 \sqrt{T/T_0} \text{ m s}^{-1}$
Density: $\rho = 1.2929 T_0/T \text{ kg m}^{-3}$
Viscosity: $\mu = 1.708 e - 5(1 + 0.0029 t) \text{ kg m}^{-1}\text{s}^{-1}$
Thermal conductivity: $\kappa = 5.77 e - 3(1 + 0.0033 t) \text{ Cal}/(\text{ms } ^\circ\text{C})$
Spec. heat with constant p.: $C_p = 240 \text{ Cal}/(\text{kg } ^\circ\text{C})$
Ratio of specific heats: $\gamma = 1.402$

Table 1: Numerical values [Chaigne and Kergomard(2016)] of air constants used in the model. t is the temperature in Celsius, and T the absolute temperature with $T_0 = 273.15^\circ \text{K}$.

frequency domain $\hat{p}(x, \omega)$ the acoustic pressure¹ 129
 and $\hat{u}(x, \omega)$ the volume flow, such that the one- 130
 dimensional interior equations read, for all position 131
 $x \in [0, L]$ and angular frequency $\omega \in [\omega_{\min}, \omega_{\max}]$, 132

$$\begin{cases} Z_v(\omega, x) \hat{u} + \frac{d\hat{p}}{dx} = 0, & (1a) \\ Y_t(\omega, x) \hat{p} + \frac{d\hat{u}}{dx} = 0, & (1b) \end{cases}$$

$$(2) \begin{cases} Z_v(\omega, x) = \frac{j\omega\rho}{S(x)} [1 - \mathcal{J}(k_v(\omega)R(x))]^{-1}, \\ Y_t(\omega, x) = \frac{j\omega S(x)}{\rho c^2} [1 + (\gamma - 1)\mathcal{J}(k_t(\omega)R(x))], \end{cases}$$

$$k_v(\omega) = \sqrt{j\omega \frac{\rho}{\mu}}, \quad k_t(\omega) = \sqrt{j\omega \rho \frac{C_p}{\kappa}},$$

where R is the section radius, $S = \pi R^2$ is the section area, table 1 describes the air constants, and we introduce the function \mathcal{J} of a complex variable, which models the dissipative terms, as

$$\mathcal{J}(z) = \frac{2 J_1(z)}{z J_0(z)}, \quad \forall z \in \mathbb{C}, \quad (3)$$

where J_0 and J_1 are the Bessel functions of the first 133
 kind. The subscripts v and t respectively stand for 134
 viscous and thermal dissipative phenomena. 135

Furthermore, if the dissipative terms are neglected 136
 (\mathcal{J} function set to zero in the equations), the classical 137
 horn equations describing plane wave propagation in 138
 an axisymmetric lossless pipe can be retrieved from 139
 an asymptotic analysis from Euler's equations in a 140
 pipe with a slowly varying section [Rienstra(2005)]. 141
 For convenience, we will use the names lossy model 142
 for system (1), and lossless model when \mathcal{J} is set to 143
 zero in system (1). 144

Two boundary conditions complete the problem: at the bell $x = L$, we impose a radiation impedance condition [Rabiner and Schafer(1978), Dalmont et al.(2001),

¹variables with a hat ($\hat{\cdot}$) denote the time-domain Fourier transform of the unknown

Chaigne and Kergomard(2016)]:

$$\frac{\hat{p}(L, \omega)}{\hat{u}(L, \omega)} = Z_R(\omega), \quad (4)$$

and at the input of the pipe, we impose $\hat{u}(0, \omega) = \lambda(\omega)$, where $\lambda(\omega)$ will be a source term for the system. Since all the considered equations are linear, we can consider without loss of generality $\lambda(\omega) \equiv 1$. In this article, we are interested in computing the input impedance

$$Z(\omega) := \frac{\hat{p}(0, \omega)}{\hat{u}(0, \omega)} = \hat{p}(0, \omega). \quad (5)$$

Finally, the considered problem is the following: compute

$$Z(\omega) = \hat{p}(0, \omega), \quad \text{where} \quad (6)$$

$$\begin{cases} \left\{ \begin{array}{l} Z_v(\omega, x) \hat{u} + \frac{d\hat{p}}{dx} = 0, \\ Y_t(\omega, x) \hat{p} + \frac{d\hat{u}}{dx} = 0, \end{array} \right. & \forall x \in [0, L] \end{cases} \quad (7a)$$

$$\hat{u}(0, \omega) = 1, \quad (7b)$$

$$\frac{\hat{p}(L, \omega)}{\hat{u}(L, \omega)} = Z_R(\omega). \quad (7c)$$

In the subsequent sections, we are interested in possible methods to solve system (7). We will first present the Finite Element Method and then the Transfer Matrix Method.

3 Finite element method

The finite element method (FEM) relies on a variational formulation of the entire system in usual infinite dimensional Sobolev spaces [Brezis(2011)], followed by the definition of finite dimensional spaces in which we seek numerically the solution. For first order formulations as the one of system (7) (flow / pressure), the theory [Courant and Hilbert(1965)] points towards the possible following framework. Find $\hat{p}_h \in V_h \subset H^1([0, L])$, $\hat{u}_h \in W_h \subset L^2([0, L])$, such that for all $q_h \in V_h$, $w_h \in W_h$,

$$\left\{ \begin{array}{l} \int_0^L \frac{j\omega\rho}{S} [1 - \mathcal{J}(k_v(\omega)R)]^{-1} \hat{u}_h w_h \\ \quad + \int_0^L \frac{d\hat{p}_h}{dx} w_h = 0 \end{array} \right. \quad (8a)$$

$$\left\{ \begin{array}{l} \int_0^L \frac{j\omega S}{\rho c^2} [1 + (\gamma - 1)\mathcal{J}(k_t(\omega)R)] \hat{p}_h q_h - \int_0^L \frac{dq_h}{dx} \hat{u}_h \\ \quad - q_h(0) + \frac{1}{Z_R(\omega)} \hat{p}_h(L) q_h(L) = 0 \end{array} \right. \quad (8b)$$

where by-parts integrations of Equations (7a) have been performed, followed by the use of the boundary conditions to weakly give a value to $\hat{u}_h(0)$ and $\hat{u}_h(L)$.

In practice, the spaces V_h and W_h are defined as follows. The instrument is discretized into N elements $\{K_j\}_j$, delimited by $N + 1$ nodes that constitute the mesh. On each element K_j we consider $r + 1$ interior degrees of freedom called $\{\xi_{j,p}\}_{1 \leq p \leq r+1}$.

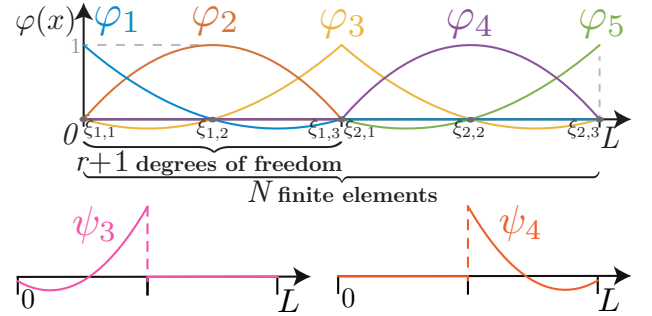


Figure 2: Basis functions with respect to x on a 2-elements mesh of $[0, L]$. Top : second order basis function $\{\varphi_i\}_{1 \leq i \leq 5}$ of V_h . Bottom : basis functions ψ_3 and ψ_4 of W_h . (colors online)

The finite dimensional spaces V_h and W_h are spanned by the nodal bases $\{\varphi_i\}_{1 \leq i \leq N_{H^1}}$ and $\{\psi_j\}_{1 \leq j \leq N_{L^2}}$ of piecewise polynomial functions of degree r (see an example of order 2 in Figure 2). They are interpolation Lagrange polynomials associated to the concatenation of all the degrees of freedom of all the elements, where the nodes separating two elements are duplicated for W_h but not for V_h . Consequently, the basis functions of V_h are continuous while the ones of W_h present a discontinuity at the edges of the elements. Moreover, $N_{H^1} < N_{L^2}$ as soon as the mesh is composed of more than two elements. Finally, the integral terms in Equations (8) are evaluated through a quadrature procedure [Quarteroni et al.(2007)]. Although a high order quadrature formula could be employed to ensure exact integration, we have chosen to follow the procedure of spectral high order finite elements [Cohen(2004)] which consists in choosing Gauss-Lobatto points as both the interpolation and quadrature points, and which leads to a diagonal mass matrix without any consistency loss. Approximate integrals that come from this procedure will be denoted f .

Since system 8 stands for every $w_h \in W_h$ and $q_h \in V_h$, it is equivalent to state that it stands for every basis vector of W_h and V_h . Besides, we abusively still denote u_h (resp. p_h) for the coordinates of u_h (resp. p_h) in the basis $\{\varphi_i\}_{1 \leq i \leq N_{H^1}}$ (resp. $\{\psi_j\}_{1 \leq j \leq N_{L^2}}$). Consequently, the discrete formulation equivalently takes the matrix form

$$\begin{cases} j\omega M_h^{L^2} \hat{u}_h + j\omega N_h^{L^2}(\omega) \hat{u}_h - B_h \hat{p}_h = 0 \end{cases} \quad (9a)$$

$$\begin{cases} j\omega M_h^{H^1} \hat{p}_h + j\omega N_h^{H^1}(\omega) \hat{p}_h + \frac{1}{Z_R(\omega)} \Sigma_h \hat{p}_h \\ \quad + B_h^* \hat{u}_h - E_h = 0 \end{cases} \quad (9b)$$

where

$$\begin{aligned} (M_h^{L^2})_{i,j} &= \int_0^L \frac{\rho}{S} \psi_i \psi_j, & (M_h^{H^1})_{i,j} &= \int_0^L \frac{S}{\rho c^2} \varphi_i \varphi_j, \\ (N_h^{L^2})_{i,j}(\omega) &= \int_0^L \frac{\rho}{S} \frac{\mathcal{J}(k_v(\omega)R)}{1 - \mathcal{J}(k_v(\omega)R)} \psi_i \psi_j, \\ (N_h^{H^1})_{i,j}(\omega) &= \int_0^L \frac{S}{\rho c^2} (\gamma - 1) \mathcal{J}(k_t(\omega)R) \varphi_i \varphi_j, \\ (B_h)_{i,j} &= - \int_0^L \psi_i \frac{d\varphi_j}{dx}, & (E_h)_i &= \varphi_i(0), \\ (\Sigma_h)_{i,j} &= \varphi_i(L) \varphi_j(L) \end{aligned}$$

Notice that $M_h^{L^2}$, $M_h^{H^1}$, $N_h^{L^2}(\omega)$, $N_h^{H^1}(\omega)$ and Σ_h are diagonal matrices, B_h is block diagonal and E_h is a vector with only one non zero entry. This discrete formulation defines the following linear system on the global unknown U_h :

$$\begin{aligned} A_h(\omega)U_h(\omega) &= L_h, & A_h(\omega) &= \begin{pmatrix} A_{11}(\omega) & A_{12}(\omega) \\ A_{21}(\omega) & A_{22}(\omega) \end{pmatrix}, \\ L_h &= \begin{pmatrix} 0 \\ E_h \end{pmatrix}, & U_h(\omega) &= \begin{pmatrix} \hat{u}_h \\ \hat{p}_h \end{pmatrix}(\omega) \end{aligned} \quad (10)$$

$$\begin{aligned} A_{11}(\omega) &= j\omega M_h^{L^2} + j\omega N_h^{L^2}(\omega) \\ A_{12}(\omega) &= -B_h, & A_{21}(\omega) &= B_h^* \\ A_{22}(\omega) &= j\omega M_h^{H^1} + j\omega N_h^{H^1}(\omega) + \frac{1}{Z_R(\omega)}\Sigma_h \end{aligned}$$

Notice that the matrix A_h is sparse and can therefore be inverted by using efficient sparse routines [scipySparse]. Once this system is numerically solved, for a discrete set of values $\{\omega_i\}_{1 \leq i \leq N_\omega} \in [\omega_{min}, \omega_{max}]$, the input impedance is

$$\forall 1 \leq i \leq N_\omega, \quad Z_{FEM}(\omega_i) = L_h^* U_h(\omega_i), \quad (11)$$

which is the $(N_{L^2}+1)$ th term of the vector $U_h(\omega_i)$.

It is possible to diminish the computational burden by performing some pre-computations based on the pipe geometry and propagation hypotheses, and by taking advantage of the geometrical and arithmetical structure of the matrix A_h and of the required output [Amestoy et al.(2000)], but this is out of the scope of the current article.

Finally, for a given frequency, the N_{L^2} first terms of U_h give an approximation of the velocity at every degree of freedom along the bore, while the N_{H^1} last terms give an approximation of the pressure.

The FEM presented in this paper is implemented in OpenWind [OpenWind], an open source Python 3 toolbox.

4 Transfer matrix method

The transfer matrix method (TMM) consists in writing relations between output and input acoustic variables of simple geometries (cylinders, cones, Bessel

and exponential bores...) from the use of the propagation equations [Caussé et al.(1984)]. Consequently, given a radiation impedance $Z_R(\omega)$ and discretizing the bore profile in a series of N_p parts, it is possible to compute the instrument's input impedance. Let $\{x_i\}_{0 \leq i \leq N_p}$ be the list of positions on the bore's axis defining all the parts (with $x_0 = 0$ and $x_{N_p} = L$). We also define $\hat{p}_i(\omega)$ and $\hat{u}_i(\omega)$ as approximations of the pressure and the volume flow calculated by the TMM at the positions x_i . When the TMM is exact, $\hat{p}_i(\omega) = \hat{p}(x_i, \omega)$ and $\hat{u}_i(\omega) = \hat{u}(x_i, \omega)$.

Formally, the relation between the input and the output of one part can be expressed as a 2×2 matrix $T_{i+1}(\omega)$:

$$\begin{aligned} \begin{pmatrix} \hat{p}_i(\omega) \\ \hat{u}_i(\omega) \end{pmatrix} &= \begin{pmatrix} a_{i+1}(\omega) & b_{i+1}(\omega) \\ c_{i+1}(\omega) & d_{i+1}(\omega) \end{pmatrix} \begin{pmatrix} \hat{p}_{i+1}(\omega) \\ \hat{u}_{i+1}(\omega) \end{pmatrix} \\ &= T_{i+1} \begin{pmatrix} \hat{p}_{i+1}(\omega) \\ \hat{u}_{i+1}(\omega) \end{pmatrix}. \end{aligned} \quad (12)$$

We then deduce the relation between the input and the output of the pipe:

$$\zeta = \begin{pmatrix} \hat{p}_0(\omega)/\hat{u}_L(\omega) \\ \hat{u}_0(\omega)/\hat{u}_L(\omega) \end{pmatrix} = \prod_{i=1}^{N_p} T_i(\omega) \begin{pmatrix} Z_R(\omega) \\ 1 \end{pmatrix}. \quad (14)$$

where $\hat{u}_L(\omega)$ is the volume flow at the pipe end, and finally $Z_{TMM} = \frac{\zeta(1)}{\zeta(2)}$. The global transfer matrix is defined as the product of all the elementary matrices T_i . An implicit transmission condition is therefore assumed, which is the continuity of the variables between all parts. In practice, the computation is done only for a discrete set of pulsations $\{\omega_j\}_{1 \leq j \leq N_\omega}$. In the sequel, we will only consider the TMM for cylinders and cones. Transfer matrices for other geometries are available in the literature [Braden(2007), Chaigne and Kergomard(2016), Helie(2013)].

For the lossless propagation case, the equations can be solved analytically for cones and cylinders and therefore the TMM provides the exact input impedance. In the presence of viscothermal losses, the bore radius is a parameter of the nonlinear dissipation terms, see Equation (2). It turns out that exact matrices can only be derived for the cylinder and not for more complex parts for which the radius depends on the space variable ($\hat{p}_i(\omega) \neq \hat{p}(x_i, \omega)$). A first empirical approach handles this difficulty for conical parts by approximating them as a succession of cylinders of increasing or decreasing radii [Caussé et al.(1984)]. A second empirical approach proposes to discretize each conical part in N_{sub} smaller cone subdivisions, and to use on each subdivision the transfer matrix derived for the cone considering lossless propagation, replacing some parameters by their lossy counterparts [Chabassier and Tournemenne(2019)] evaluated at a chosen intermediate radius R^\odot [Mapes-Riordan(1993), Braden(2007)]. For

255 a bore initially made of N_p conical parts, the total
 256 number of actual transfer matrices to compute would
 257 be $N_{\text{TMM}} = N_p \times N_{\text{sub}}$.

258 Since the viscothermal losses depend non-linearly
 259 on the radius, no optimal value for R^\odot can be im-
 260 mediately derived. Possible choices are the average
 261 radius $R^\odot = (R_i + R_{i+1})/2$ [Mapes-Riordan(1993)]
 262 (where R_i and R_{i+1} are the input and output radii
 263 of the cone subdivision), or any other weighted aver-
 264 age [Chaigne and Kergomard(2016), Helie(2013)]. In
 265 this article, we choose $R^\odot = (2 \min(R_i, R_{i+1}) +$
 266 $\max(R_i, R_{i+1}))/3$, which seems to be used in some
 267 existing implementations of the TMM.

We have shown [Chabassier and Tournemene(2019)]
 that using the TMM with the approximate matrix
 obtained with this strategy corresponds to actually
 solving analytically the following system of equations:

$$Z_{\text{TMM}}(\omega) = \check{p}(0, \omega), \text{ where } \forall i \in [1, N_{\text{TMM}}], \quad (15)$$

$$\left\{ \begin{array}{l} Z_v^i \check{u} + \frac{d\check{p}}{dx} = 0, \\ Y_t^i \check{p} + \frac{d\check{u}}{dx} = 0, \end{array} \quad \forall x \in [x_i, x_{i+1}] \quad (16a)$$

$$Z_v^i = \frac{j\omega \rho}{S} [1 - \mathcal{J}(k_v(\omega)R_i^\odot)]^{-1}, \quad (16b)$$

$$Y_t^i = \frac{j\omega S}{\rho c^2} [1 + (\gamma - 1)\mathcal{J}(k_t(\omega)R_i^\odot)], \quad (16c)$$

$$\check{p}(x_{i-}) = \check{p}(x_{i+}), \quad \check{u}(x_{i-}) = \check{u}(x_{i+}), \quad (16d)$$

$$R_i^\odot = (2 \min(R(x_i), R(x_{i+1})) + \max(R(x_i), R(x_{i+1}))) / 3, \quad (16e)$$

$$\check{u}(0, \omega) = 1, \quad (16f)$$

$$\frac{\check{p}(L, \omega)}{\check{u}(L, \omega)} = Z_R(\omega). \quad (16g)$$

268 This problem is different from the continuous prob-
 269 lem (7) solved with the FEM. The difference lies in
 270 the approximation R^\odot inside the function \mathcal{J} for every
 271 interval $[x_i, x_{i+1}]$ and amounts to approximating the
 272 original equation coefficients with discontinuous ones.

Finally, we propose a unified formulation for the
 computation of the transfer matrix $T_{i+1}(\omega)$, equal to
 the one of the literature [Mapes-Riordan(1993)], for
 cones and cylinders under visco-thermal losses. It
 reads:

$$a_{i+1}(\omega) = a, \quad b_{i+1}(\omega) = b, \quad c_{i+1}(\omega) = c, \quad d_{i+1}(\omega) = d,$$

where

$$(17) \left\{ \begin{array}{l} a = \frac{R_{i+1}}{R_i} \cosh \Gamma \ell - \frac{\beta}{\Gamma} \sinh \Gamma \ell \\ b = \frac{R_i}{R_{i+1}} Z_c \sinh \Gamma \ell \\ c = \frac{1}{Z_c} \left[\left(\frac{R_{i+1}}{R_i} - \frac{\beta^2}{\Gamma^2} \right) \sinh \Gamma \ell + \frac{\beta^2 \ell}{\Gamma} \cosh \Gamma \ell \right] \\ d = \frac{R_i}{R_{i+1}} \left(\cosh \Gamma \ell + \frac{\beta}{\Gamma} \sinh \Gamma \ell \right) \end{array} \right.$$

where

$$\Gamma \equiv \Gamma(\omega, R^\odot) = \frac{j\omega}{c} \sqrt{\frac{1 + (\gamma - 1)\mathcal{J}(k_t(\omega)R_i^\odot)}{1 - \mathcal{J}(k_v(\omega)R_i^\odot)}},$$

$$Z_c \equiv Z_c(\omega, R^\odot) = \frac{\rho c}{S(x_i)} \sqrt{\frac{[1 + (\gamma - 1)\mathcal{J}(k_t(\omega)R_i^\odot)]^{-1}}{1 - \mathcal{J}(k_v(\omega)R_i^\odot)}}$$

and

$$\beta = \frac{R_{i+1} - R_i}{\ell R_i}, \quad (18)$$

where R_i and R_{i+1} are respectively the input and out-
 put radii of the interval, ℓ is the axial length of the
 interval, and R^\odot the previously defined quantity.

The transfer matrices for cylinders and cones in the
 lossless case can be similarly unified, it only requires
 to replace Γ by $j\omega/c$ and Z_c by $\rho c/S$.

The TMM presented in this paper is implemented
 in OpenWind [OpenWind].

5 Results

Unless otherwise stated, all input impedances pre-
 sented hereafter are numerically computed from 20
 to 2000 Hz with a 1Hz step, the temperature is
 set to 25 °C, and we consider a final impedance
 that models radiation from an infinite plane baf-
 fle [Rabiner and Schafer(1978)]:

$$Z_R(\omega) = \frac{\rho c}{S(L)} \frac{j\omega}{\alpha + j\omega\beta}, \quad (19)$$

where $\alpha = 3c\pi/(8R)$ and $\beta = 9\pi^2/128$. Other flanges
 can be modelled with this impedance form, by ad-
 justing consequently the coefficients α and β , with
 a corresponding frequency validity range. Any other
 choice of radiation impedance can be done, including
 experimental ones, provided that the associated sys-
 tem of equations is well posed, meaning that its real
 part must be non-negative [Chandler-Wilde(1997)].
 The discussion about radiation impedances is out of
 the scope of this paper, but it is important to note
 that the following conclusions regarding convergence
 rates and accuracy do not depend on this choice.

In the following, the FEM meshes are constructed
 as follows. A target element size (TES) is chosen by
 the user. The instrument being described by a series
 of radii at different axial points, some of the instru-
 ment parts might be shorter than the TES, and some
 might be longer. The instrument parts longer than
 the TES are equally divided to only obtain elements
 smaller or equal to the TES. Notice that when the
 user chooses a TES bigger than the smallest instru-
 ment part, some elements will be smaller than the
 TES, which provides a non-uniform mesh. Moreover,
 for realistic instruments, any TES choice will produce
 a non-uniform mesh since the instrument parts are
 not necessarily commensurate. The ratio τ between

the largest and smallest elements in a mesh is an indicator of this uniformity, and is equal to 1 for a uniform mesh.

Up to 8 geometries are studied in the following. One 20 cm cylinder with 5 mm radius (roughly corresponding to a trumpet leadpipe) is used to assess an error estimator for the lossy model. We use 5 different cones and one arbitrary simple discontinuous geometry to help analyze the TMM error for the lossy model, and one trumpet-like bore for a realistic study of the lossless and lossy models. The cones share their dimensions with existing instruments or instruments parts, and the trumpet is made of 9 cones to describe the mouthpiece, 4 cones for the leadpipe, 1 central cylinder and 20 cones for the bell (33 cones in total). Apart from the cylinder, the 7 other geometries are described in Figure 3. Notice that the 3 cones corresponding to the mouthpiece cup, backbore, and the trumpet leadpipe parts would normally be inside the instrument and yet we consider here their input impedance with open air radiation.

Notice that the relative errors that will be considered in the following of this paper are consequent to the discretization of the equations, and must be distinguished from the model error that would induce a discrepancy between the simulations and physical experiments. Quantifying this discretization error allows to correctly interpret the results of simulations.

All the results are obtained with OpenWind [OpenWInD].

5.1 Case without dissipation

The TMM is numerically exact for the lossless model, and can therefore be taken as a reference in this case. Consequently, in order to assess the numerical quality of the FEM, we compute the relative error of the FEM solution to the reference solution obtained with the TMM, E_{TMM} , in the lossless case, defined as:

$$E_{\text{TMM}}(i) = \frac{\|Z_{i \text{ FEM}} - Z_{\text{TMM}}\|}{\|Z_{\text{TMM}}\|}, \quad (20)$$

where $Z_{i \text{ FEM}}$ is the impedance computed using the FEM at order i , and Z_{TMM} the impedance computed using the TMM, and $\|\cdot\|$ denotes the discrete ℓ^2 norm of a vector over all the considered frequencies.

The upper part of Figure 4 shows the logarithm of $E_{\text{TMM}}(i)$ with respect to the order i of the FEM for the specific case of the trumpet bore displayed in Figure 3.

The mesh is obtained by choosing a TES equal to 3.4 cm, which gives $N = 72$ elements, with a ratio $\tau = 17$. We observe that the FEM provides a solution that is closer and closer to Z_{TMM} as the order increases. After order 10 (which represents a total of 649 degrees of freedom for the H^1 variable, 1369 degrees of freedom in total), the impedance relative ℓ^2

error does not diminish anymore and is close to 2.6e-12, which is dominated by roundup errors in double precision as expected. In the sequel we will call this a “converged solution”. The linear convergence in logarithmic scale agrees with the finite elements theory which predicts an exponential order (spectral) convergence. The lower part of Figure 4 shows the logarithm of $E_{\text{TMM}}(i)$ with respect to the logarithm of the target element size (TES) of the mesh, for the different FEM orders 1 to 6. Since the trumpet bore is composed of very large and very small parts, the observed curves are not yet exhibiting asymptotic rates of convergence (we would need much smaller TES in this case). However, we observe that for a given TES (and therefore mesh), increasing the order of the FEM always diminishes the relative ℓ^2 error on the input impedance, achieving a precision that is difficult to reach by refining the mesh at a given order.

5.2 Case with dissipation

Regarding the model with viscothermal losses (lossy model), the TMM is exact for cylinders only. It will thus not be possible to use E_{TMM} to assess FEM convergence towards the exact solution for geometries of arbitrary shapes. Instead, we compute the relative ℓ^2 error between two finite element computations on the same mesh but consecutive orders:

$$E_{\text{order}}(i) = \frac{\|Z_{i+1 \text{ FEM}} - Z_{i \text{ FEM}}\|}{\|Z_{i \text{ FEM}}\|}, \quad (21)$$

which is a classic error estimator.

The first considered case is a cylinder 20 cm long with a 5 mm radius, which could be compared qualitatively to a trumpet leadpipe in terms of dimensions. In Figure 5, we consider a mesh of $N = 6$ elements and we represent both the E_{TMM} and the E_{order} relative ℓ^2 error estimators, since E_{TMM} is relevant in this case (it measures the distance to an exact solution). The two error estimators exhibit a very similar behavior which illustrates the fact that they are both relevant to assess the convergence of the FEM. In this case, the FEM provides a converged solution at order 9. The fact that E_{order} tends to machine precision is completed by the usual finite elements convergence theory in order to ensure that the obtained numerical solution is actually close to the exact impedance of the considered instrument (as opposed to a converged but false numerical solution) [Dauge et al.(2005)].

Figure 6 shows the modulus of the input impedance computation for the same cylinder with respect to the frequency, for different FEM orders. The difference between the curves is visible for all orders, which is consistent with the fact that the solution is not yet converged. At a given order, the error increases with the frequency, which is known as the “pollution effect” [Gerdes and Ihlenburg(1999)]. When the order increases, the solution becomes valid in a wider frequency range. Two main effects are to be noted in the

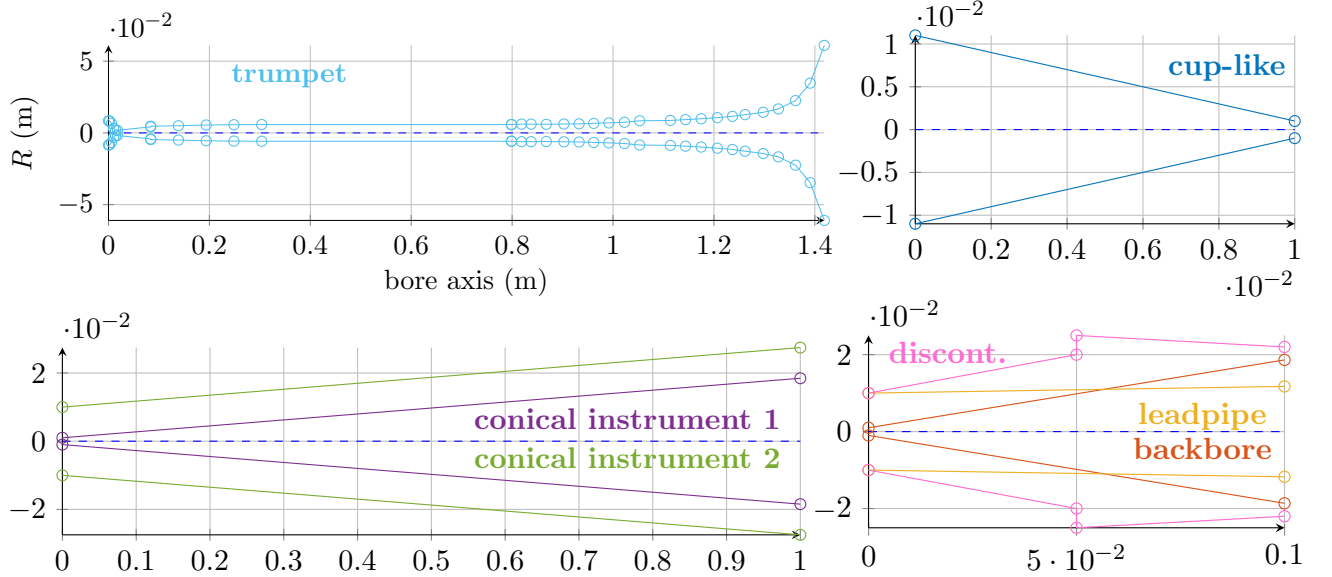


Figure 3: The seven studied bores. Top left : trumpet-like bore. Top right : simple convergent cone of general dimensions similar to a mouthpiece cup. Bottom left : two cones of 1m representative of conical instruments. Bottom right : two cones being qualitatively similar to a mouthpiece backbore and a trumpet leadpipe part, and one arbitrary geometry made of two cones, one divergent, the other convergent, and a clear discontinuity between them. The circles represent the extremities of each part. (colors online)

402 context of musical acoustics: the peaks amplitudes
 403 and frequencies can be wrong, the latter being due to
 404 numerical dispersion [Ihlenburg and Babuška(1995)].
 405 Increasing the number of elements and/or the order
 406 allow to reduce these effects down to machine pre-
 407 cision. In this case, at low orders of discretization,
 408 erroneous conclusions can be drawn if the user does
 409 not attribute the dispersion to the numerical approx-
 410 imation but to the model.

411 Notice finally that finite differences
 412 [Bilbao and Chick(2013)] can be seen, at least
 413 locally, as first order finite elements. The analyses of
 414 Figures 4 and 6 illustrate the fact that using a first
 415 order approximation can be a source of inaccuracy in
 416 the context of musical acoustics.

417 Figure 7 shows the logarithm of the consecutive rela-
 418 tive ℓ^2 error E_{order} with respect to the FEM order,
 419 considering the geometries of Figure 3, in the lossy
 420 case. The number of elements is indicated in the leg-
 421 end. An exponential order convergence is still ob-
 422 served in the presence of dissipation which is in agree-
 423 ment with the FEM theory. Depending on the case,
 424 the solution seems to be converged at an order rang-
 425 ing between 5 and 10, which is related to the prop-
 426 erties of the chosen mesh and to mathematical constants
 427 depending on the exact solution.

428 A converged FEM solution can therefore be con-
 429 sidered as the reference numerical solution for the
 430 lossy model, on geometries for which no exact solu-
 431 tion is available. As said earlier, the TMM used on
 432 the lossy model is not exact for bores of arbitrary
 433 shape, and follows an empirical approach to compute

input impedances, see section 4. In this study, we in-
 vestigate the second empirical approach, subdividing
 every conical part in N_{sub} equal segments and using
 for each subdivision the formula (17), which amounts
 to solving the approximate Equations (16).

It is possible to study the error made by the TMM
 approximation, by computing the relative ℓ^2 error
 with the converged FEM input impedance:

$$E_{\text{conv FEM}}(j) = \frac{\|Z_j \text{ TMM} - Z_{\text{conv FEM}}\|}{\|Z_{\text{conv FEM}}\|}, \quad (22)$$

where $Z_j \text{ TMM}$ is the input impedance computed us-
 ing the TMM with j subdivisions for each instru-
 ment part, and $Z_{\text{conv FEM}}$ is the converged imped-
 ance obtained by the FEM.

Since both methods solve different systems of equa-
 tions (namely, Equations (7) for the FEM and Equa-
 tions (16) for the TMM), the error between their so-
 lutions will be related to the difference between their
 equations [Chabassier and Tournemenne(2019)]. As j
 increases, the TMM equations tend to the FEM equa-
 tions and thus we expect both solutions to converge.

Figure 8 shows the logarithm of $E_{\text{conv FEM}}$ with
 respect to the logarithm of the smallest subdivision
 length Δx_j used to compute $Z_j \text{ TMM}$, for the dif-
 ferent bores displayed in Figure 3. The relative error
 is computed on a frequency range of [20, 2000] Hz
 with a 1Hz step, but the obtained results are sim-
 ilar when a different frequency range is considered.
 A first observation is that all curves are decreasing
 at rate close to 1 asymptotically (error divided by
 10 when the subdivisions length is divided by 10).
 For the first conical

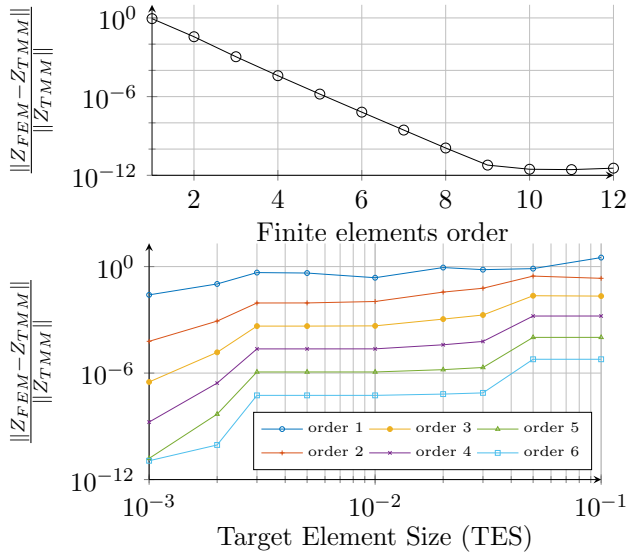


Figure 4: Relative ℓ^2 error between the input impedance obtained with the FEM and the TMM for the trumpet under lossless conditions. Top: the finite elements order varies on a given mesh, Bottom: the target element size (TES) varies for different FEM orders. (colors online)

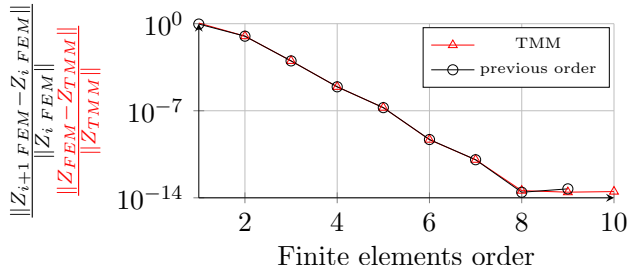


Figure 5: Comparison between E_{order} and E_{TMM} for a 20 cm cylinder of radius 5 mm using the lossy model. The FEM mesh is uniform with 3 elements.

463 instrument, the mouthpiece backbore and more extensively, for the cup-like bore, the curves show a dip
 464 for a specific subdivision length value. This can happen when considering few subdivisions for each cone
 465 and disappears asymptotically, and can be interpreted as fortuitous values of R^\odot for the cones subdivisions.
 466 More quantitatively, the error $E_{\text{conv FEM}}$ illustrates the difference between the discretized TMM approach
 467 problem (16) and the original system (7). Because the convergence is slow (order 1 w.r.t. the subdivision
 468 length), the number of TMM subdivisions needed to obtain a solution that has converged up to machine
 469 precision is very large and induces a very heavy computational cost.

477 Figure 9 shows the input impedance of the instrument Conical inst. 1 on the frequency range $[0, 2]$
 478 kHz and $[1120, 1150]$ Hz (close to the 7th impedance peak). On this example, the amplitude and frequency
 479 position of the impedance peaks are misjudged by the
 480
 481

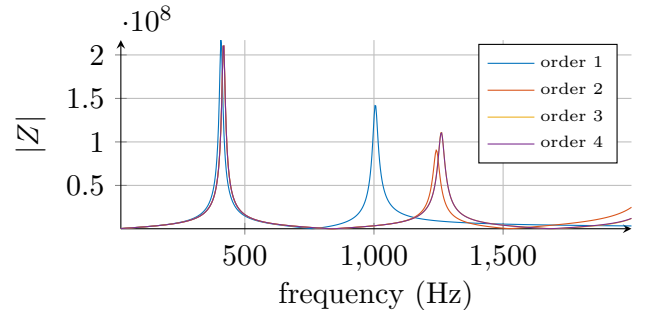


Figure 6: Modulus of the input impedance of a 20 cm cylinder of radius 5 mm computed by the FEM at different orders. (colors online)

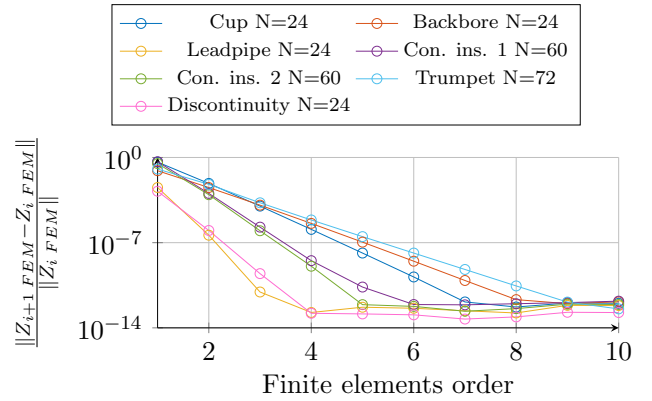


Figure 7: Consecutive relative ℓ^2 error between the input impedances obtained with the FEM for the lossy model using the bores of Figure 3 with respect to the FEM order. The number of elements of each mesh is given in the legend for each geometry. (colors online, matching with Figure 3)

TMM when the number of subdivisions is too low. 482
 For example, the height of the 7th peak of this instrument is 6.9% too low ($3.56e8$ against $3.32e8$) when 483
 considering a subdivision length of 0.17 m (6 subdivisions), and its frequency position is 1.37 cents too low 484
 (1136Hz against 1135Hz). In the case of the cup-like bore, this frequency shift is even higher (4.99 cents 485
 for the first peak around 2000Hz with a subdivision length of 0.01 m (1 subdivision) for the TMM). 486
 487
 488
 489
 490

5.3 Computation time and features comparison of the two approaches 491

Computation time In the previous paragraphs, 493
 we have seen that both the FEM and the TMM are relevant to compute the input impedance of a given 494
 instrument as defined in Equations (7). In order to complete the methods' performance analysis, it is necessary 495
 to assess and compare their computational costs. Fast input impedance computation is especially useful 496
 when considering optimization applications where a large number of input impedances must be com- 497
 498
 499
 500
 501

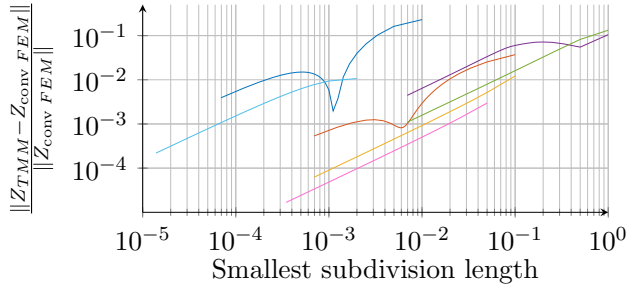


Figure 8: Relative ℓ^2 error between TMM solution and the converged FEM solution for the bores of Figure 3, w.r.t. the smallest subdivision length used for the TMM computation. (colors online, matching with Figure 3)

502 puted to reach optimal designs. Recall that the FEM
 503 computation requires the inversion of the sparse linear
 504 system (10) while the TMM computation requires
 505 the evaluation of the matrices product (14), both for a
 506 discrete set of pulsations $\{\omega_i\}_{1 \leq i \leq N_\omega}$. A fair compar-
 507 ison can only be performed for numerical solutions
 508 that provide the same precision with respect to the
 509 exact solution. Since the FEM relies on the choice
 510 of both a mesh and an order, the same precision can
 511 be obtained with several situations that do not nec-
 512 essarily induce the same computational cost. In the
 513 sequel, the given time is always the smallest found
 514 computational time.

515 Firstly, for the cases where the TMM are exact
 516 (lossless case, lossy cylinder), the TMM computation
 517 is very competitive and provides the exact solution
 518 with only roundup errors. On the contrary, the FEM
 519 needs to be converged in order to provide a solution
 520 with a similar precision, and this induces an extra
 521 computational cost (about 1883 times more for the
 522 lossless trumpet and 194 times more for the lossy
 523 cylinder).

524 In the presence of viscothermal losses and arbitrary
 525 shapes, the TMM is not exact anymore and uses a dis-
 526 crete and empirical approach to compute the input
 527 impedance. We display in Figure 10 the computation
 528 times with respect to the relative ℓ^2 error to the con-
 529 verged solution, for the realistic trumpet-like bore²,
 530 for several TMM subdivision lengths (from $\Delta x = 2e$ -
 531 $3m$ to $1.3e$ - $5m$) and for the FEM with 35 elements
 532 at order 4. Another FEM strategy called “adaptive” is
 533 also considered: it adapts the order of each mesh ele-
 534 ment to its size. This strategy avoids introducing too
 535 many degrees of freedom in small elements, improving
 536 the computation time without diminishing the global
 537 ℓ^2 error. In the example of Figure 10, the adaptive
 538 FEM improves the computation time by 15.8% com-
 539 pared with the usual FEM, and both computations
 540 lead to a relative ℓ^2 error of 4.1×10^{-4} .

²Computations run on a 3.4GHz Intel Core i7-2600 with 16 GB of RAM

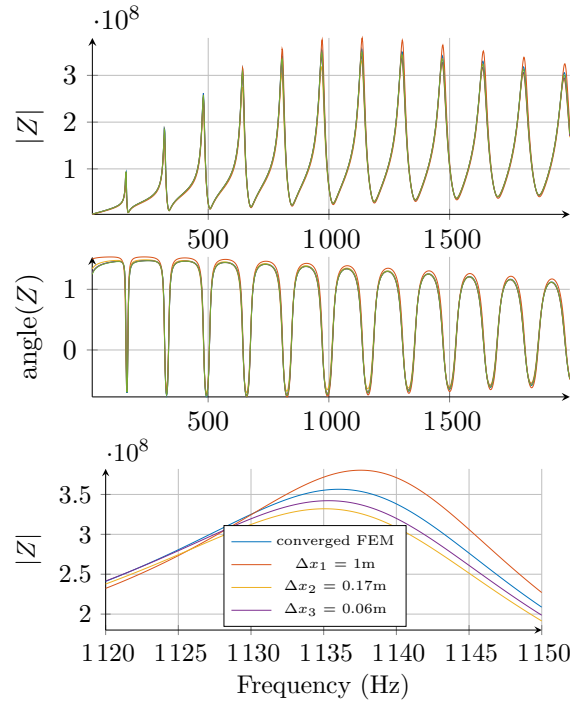


Figure 9: Impedance comparison between the converged FEM and the TMM method using different subdivision lengths of the Conical instrument 1. (colors online)

The fastest TMM setting ($\Delta x = 2e$ - $3m$), provides a
 541 relative ℓ^2 error equal to 1.1% and computes the input
 542 impedance in 0.225 seconds, which is 12 times faster
 543 than the adaptive FEM (2.7 seconds). The most
 544 precise TMM setting has a precision similar to the
 545 FEM (2.2×10^{-4}), but the computation time is 11.1
 546 times higher than the adaptive FEM (30.1s). This
 547 shows the overall numerical performance of the FEM,
 548 which can target a specific precision while maintaining
 549 a competitive computation time. 550

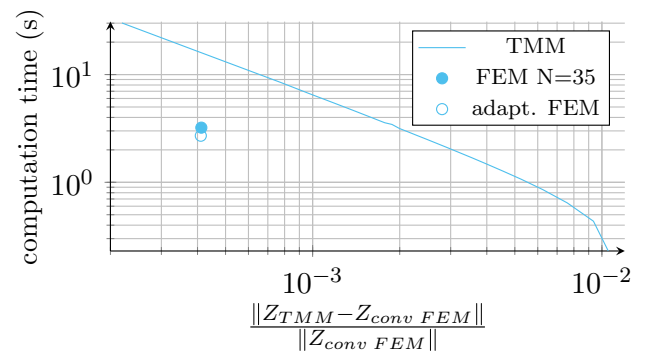


Figure 10: CPU time of the trumpet impedance computation w.r.t impedance relative ℓ^2 error. Comparison between the TMM and FEM methods.

Acoustic variables One immediate feature per-
 551 mitted by the FEM is the availability of the pressure 552

553 and volume flow spectra along the entire bore axis,
 554 see Figure 11, which is directly obtained by consider-
 555 ing all the vector U_h of system (10) (and not only the
 556 term corresponding to the entry pressure). This out-
 557 put therefore comes at no extra computational cost
 558 compared to the impedance computation. It could
 559 also be possible to reconstruct the pressure and vol-
 560 ume flow using the TMM, but it would induce extra
 561 computational cost due to over sampling of the bore
 562 profile. With non negligible extra efforts regarding
 563 the parameterization of the bore profile, it could also
 564 be possible to reconstruct the pressure and volume
 flow using the TMM.

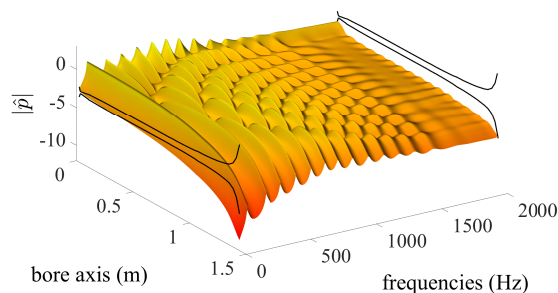


Figure 11: Evolution of the pressure modulus in logarithmic scale along the bore of the lossy trumpet according to frequency. The border at the beginning of the instrument (bore axis $x = 0$) displays the input impedance. (colors online)

565 In the case of a wind instrument, it helps to under-
 566 stand where the nodes and antinodes of the waves are
 567 located, which may help instrument makers better vi-
 568 sualize the instrument’s functioning or even position
 569 the toneholes³.
 570

571 **Extended physical situations** One major advan-
 572 tage of using FEM over TMM is the possibility to
 573 easily solve equations with no available analytical
 574 solution, which potentially gives access to instru-
 575 ments impedances in very interesting physical situa-
 576 tions. For instance, it is theoretically and technically
 577 straightforward to consider non-constant physical co-
 578 efficients, as in the case where the temperature varies
 579 inside the pipe. Figure 12 shows the modulus of the
 580 input impedance of the trumpet for a linear tempera-
 581 ture gradient [Gilbert et al.(2006)] between 37 and 21
 582 °C, and an averaged temperature of 29 °C inside the
 583 bore. There is a 7% difference between the two mod-
 584 uli, showing the importance of the temperature gra-
 585 dient for impedance calculation. Other possibilities
 586 include the accurate consideration of arbitrary bores
 587 (Bessel, exponential, polynomials, splines, ...), the
 588 possible integration of new terms in the equations or

³private discussion with the instrument maker Augustin Humeau

the coupling with other equations modelling different
 physical phenomena (pipes junctions, or excitators as
 lips, reeds, flue, ...).

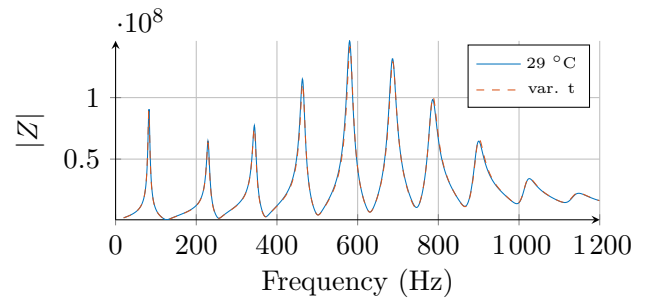


Figure 12: Impedance comparison between a constant temperature inside the bore and a linear temperature gradient from 37 to 21 °C for the trumpet bore. (colors online)

6 Conclusion and prospects

In realistic cases as a trumpet with losses, the FEM allows to compute the same numerical solution as the TMM with a limited computational cost. It also allows to compute unusual physical situations as non-constant coefficients along the bore. Moreover, the computation gives a direct access to the acoustic variables inside the pipe for no extra computational cost or over-sampling. All the results of this article have been computed and can be run again using the open-source python toolbox OpenWind [OpenWInD]. Two direct extensions can follow this work: the implementation of toneholes in the model in order to model the input impedance of woodwind instruments, and the sound synthesis based on the same finite element method in space and finite difference in time. Notice that the presence of visco-thermal terms induces a major theoretical difficulty in the time domain [Berjamin et al.(2017)]. Finally this finite element framework is an efficient basis aiming at developing an inversion algorithm based on the full-waveform inversion [Virieux and Operto(2009)]. This technique can be used to optimize the instrument’s geometry based on criteria derived from the input impedance, and relies strongly on the additional outputs of the FEM impedance computation which are the pressure and flow fields inside the instrument.

References

- [scipySparse] “<https://docs.scipy.org/doc/scipy/reference/sparse.html>” .
- [OpenWInD] “<https://gitlab.inria.fr/openwind/release>” .

- 624 [Amestoy et al.(2000)] Amestoy, P. R., Duff, I., and
625 L'Excellent, J.-Y. (2000). "Multifrontal par-
626 allel distributed symmetric and unsymmetric
627 solvers," *Comput. Methods in Appl. Mech. Eng.*
628 **184**, 501–520.
- 629 [Backus(1976)] Backus, J. (1976). "Input impedance
630 curves for the brass instruments," *The Journal*
631 *of the Acoustical Society of America* **60**(2), 470–
632 480.
- 633 [Berjamin et al.(2017)] Berjamin, H., Lombard, B.,
634 Vergez, C., and Cottanceau, E. (2017). "Time-
635 Domain numerical modeling of brass instruments
636 including nonlinear wave propagation, viscother-
637 mal losses, and lips vibration," *Acta Acust*
638 *united Ac* **103**(1), 117–131.
- 639 [Bilbao(2009)] Bilbao, S. (2009). "Direct simulation
640 of reed wind instruments," *Computer Music*
641 *Journal* **33**(4), 43–55.
- 642 [Bilbao and Chick(2013)] Bilbao, S., and Chick, J.
643 (2013). "Finite difference time domain simula-
644 tion for the brass instrument bore," *J. Acoust.*
645 *Soc. Am.* **134**(5), 3860–3871.
- 646 [Braden(2007)] Braden, A. C. P. (2007). "Bore opti-
647 misation and impedance modelling of brass musi-
648 cal instruments," Ph.D. thesis, University of Ed-
649 inburgh.
- 650 [Braden et al.(2009)] Braden, A. C. P., Newton,
651 M. J., and Campbell, D. M. (2009). "Trombone
652 bore optimization based on input impedance tar-
653 gets," *J. Acoust. Soc. Am.* **125**(4), 2404–2412.
- 654 [Brezis(2011)] Brezis, H. (2011). "Functional analy-
655 sis, Sobolev spaces and partial differential equa-
656 tions," (Springer New York, London).
- 657 [Buys et al.(2017)] Buys, K., Sharp, D., and Laney,
658 R. (2017). "Developing and evaluating a hybrid
659 wind instrument," *Acta Acust united Ac* **103**(5),
660 830–846.
- 661 [Campbell(2004)] Campbell, M. (2004). "Brass in-
662 struments as we know them today," *Acta Acust*
663 *united Ac* **90**(4), 600–610.
- 664 [Caussé et al.(1984)] Caussé, R., Kergomard, J., and
665 Lurton, X. (1984). "Input impedance of brass
666 musical instruments—comparison between ex-
667 periment and numerical models," *J. Acoust. Soc.*
668 *Am.* **75**(1), 241–254.
- 669 [Chabassier and Tournemene(2019)] Chabassier, J.,
670 and Tournemene, R. (2019). "About the trans-
671 fert matrix method in the context of acoustical
672 wave propagation in wind instruments," INRIA
673 Research Report 9254.
- [Chaigne and Kergomard(2016)] Chaigne, A., and
674 Kergomard, J. (2016). *Modern Acoustics and*
675 *Signal Processing "Acoustics of Musical Instru-*
676 *ments:,"* (Springer New York). 677
- [Chandler-Wilde(1997)] Chandler-Wilde, S. N.
678 (1997). "The impedance boundary value prob-
679 lem for the Helmholtz equation in a half-plane,"
680 *Mathematical Methods in the Applied Sciences*
681 **20**, 813–840. 682
- [Cohen(2004)] Cohen, G. (2004). "Higher Order Nu-
683 merical Methods for Transient Wave Equations,"
684 (Springer, Berlin, Heidelberg). 685
- [Courant and Hilbert(1965)] Courant, R., and
686 Hilbert, D. (1965). "Methods of mathemat-
687 ical physics. partial differential equations,"
688 *Interscience* **2**. 689
- [Dalmont et al.(2001)] Dalmont, J.-P., Nederveen,
690 C. J., and Joly, N. (2001). "Radiation impedance
691 of tubes with different flanges: Numerical and ex-
692 perimental investigations," *Journal of Sound and*
693 *Vibration* **244**(3), 505 – 534. 694
- [Dauge et al.(2005)] Dauge, M., Costabel, M., and
695 Schwab, C. (2005). "Exponential convergence of
696 hp-fem for maxwell's equations with weighted
697 regularization in polygonal domains," *Math.*
698 *Models Methods Appl. Sci.* **15**(4), 575–622. 699
- [Gerdes and Ihlenburg(1999)] Gerdes, K., and Ihlen-
700 burg, F. (1999). "On the pollution effect in FE
701 solutions of the 3D-Helmholtz equation," *Com-*
702 *puter Methods in Applied Mechanics and Engi-*
703 *neering* **170**(1–2), 155–172. 704
- [Gilbert et al.(2006)] Gilbert, J., Ruiz, L. L.,
705 and Gougeon, S. (2006). "Influence de la
706 température sur la justesse d'un instrument
707 à vent," in *Proceedings of Congres Français*
708 *d'Acoustique 2006, Tours.* 709
- [Giordano(2014)] Giordano, N. (2014). "Simulation
710 studies of a recorder in three dimensions," *J.*
711 *Acoust. Soc. Am.* **135**(2), 906–916. 712
- [Helie(2013)] Hélie, Thomas and Hézard, Thomas
713 and Mignot, Rémi and Matignon, Denis (2013).
714 "One-dimensional acoustic models of horns and
715 comparison with measurements," *Acta Acust*
716 *united Ac* **99**(6), 960–974. 717
- [Ihlenburg and Babuška(1995)] Ihlenburg, F., and
718 Babuška, I. (1995). "Dispersion analysis and er-
719 ror estimation of galerkin finite element meth-
720 ods for the Helmholtz equation," *Int. J. Numer.*
721 *Methods Engrg.* **38**, 3745–3774. 722
- [Kausel(2001)] Kausel, W. (2001). "Optimization of
723 brasswind instruments and its application in bore
724

- reconstruction,” *Journal of New Music Research* **30**(1), 69–82.
- [Kirchhoff(1868)] Kirchhoff, G. (1868). “Ueber den einfluss der wärmeleitung in einem gase auf die schallbewegung,” *Annalen der Physik* **210**(6), 177–193.
- [Le Roux et al.(2008)] Le Roux, J. C., Dalmont, J.-P., and Gazengel, B. (2008). “A new impedance tube for large frequency band measurement of absorbing materials,” *J. Acoust. Soc. Am.* **123**(5), 3119.
- [Lefebvre and Scavone(2012)] Lefebvre, A., and Scavone, G. P. (2012). “Characterization of woodwind instrument toneholes with the finite element method,” *The Journal of the Acoustical Society of America* **131**(4), 3153–3163.
- [Mapes-Riordan(1993)] Mapes-Riordan, D. (1993). “Horn modeling with conical and cylindrical transmission-line elements,” *J. Audio Eng. Soc.* **41**(6), 471–484.
- [Plitnik and Strong(1979)] Plitnik, G. R., and Strong, W. J. (1979). “Numerical method for calculating input impedances of the oboe,” *The Journal of the Acoustical Society of America* **65**(3), 816–825.
- [Quarteroni et al.(2007)] Quarteroni, A., Sacco, R., and Saleri, F. (2007). “Méthodes Numériques : Algorithmes, analyse et applications,” (Springer-Verlag Mailand).
- [Rabiner and Schafer(1978)] Rabiner, L. R., and Schafer, R. W. (1978). “Digital processing of speech signals,” **100** (Prentice-hall Englewood Cliffs, NJ).
- [Rienstra(2005)] Rienstra, S. W. (2005). “Webster’s horn equation revisited,” *SIAM Journal on Applied Mathematics* **65**(6), 1981–2004.
- [Sharp et al.(2011)] Sharp, D., Mamou-Mani, A., and van Walstijn, M. (2011). “A single microphone capillary-based system for measuring the complex input impedance of musical wind instruments,” *Acta Acust united Ac* **97**(5), 819–829.
- [Silva et al.(2014)] Silva, F., Vergez, C., Guillemain, P., Kergomard, J., and Debut, V. (2014). “MoReeSC: A framework for the simulation and analysis of sound production in reed and brass instruments,” *Acta Acust united Ac* **100**(1), 126–138.
- [Tournemenne et al.(2017)] Tournemenne, R., Petiot, J.-F., Talgorn, B., Kokkolaras, M., and Gilbert, J. (2017). “Brass instruments design using physics-based sound simulation models and surrogate-assisted derivative-free optimization,” *Journal of Mechanical Design* **139**(4), 041401.
- [van den Doel and Ascher(2008)] van den Doel, K., and Ascher, U. M. (2008). “Real-time numerical solution of webster’s equation on a nonuniform grid,” *IEEE Transactions on Audio, Speech, and Language Processing* **16**(6), 1163–1172, doi: 10.1109/TASL.2008.2001107.
- [Virieux and Operto(2009)] Virieux, J., and Operto, S. (2009). “An overview of full-waveform inversion in exploration geophysics,” *Geophysics* **74**(6), WCC1–WCC26.
- [Webster(1947)] Webster, J. C. (1947). “An electrical method of measuring the intonation of cup-mouthpiece instruments,” *The Journal of the Acoustical Society of America* **19**(5), 902–906.
- [Zwicker and Kosten(1949)] Zwicker, C., and Kosten, C. W. (1949). “Sound absorbing materials,” (Elsevier).